

Communication

# Trapping an Ester Hydrate Intermediate in a $\pi$ -Stacked Macrocycle with Multiple Hydrogen Bonds

Bin Wang<sup>1,2,3,4</sup>, Zi-Ang Nan<sup>1,3</sup>, Qing Li<sup>1,3</sup>, Jin Liu<sup>1,3</sup>, Zi-Xiu Lu<sup>1,3</sup>, Wei Wang<sup>1,3</sup>, Zhu Zhuo<sup>1,3</sup>, Guo-Ling Li<sup>1,3</sup> and You-Gui Huang<sup>1,2,3,\*</sup> 

- <sup>1</sup> CAS Key Laboratory of Design and Assembly of Functional Nanostructures, and Fujian Provincial Key Laboratory of Nanomaterials, Fujian Institute of Research on the Structure of Matter, Chinese Academy of Sciences, Fuzhou 350002, China; wb@fjirsm.ac.cn (B.W.); nanzhang@fjirsm.ac.cn (Z.-A.N.); xmliqing@fjirsm.ac.cn (Q.L.); xmliujin@fjirsm.ac.cn (J.L.); zxl@mail.ustc.edu.cn (Z.-X.L.); wangwei@fjirsm.ac.cn (W.W.); zhuozhu@fjirsm.ac.cn (Z.Z.); 6469@cumt.edu.cn (G.-L.L.)
- <sup>2</sup> Fujian Science & Technology Innovation Laboratory for Optoelectronic Information of China, Fuzhou 350108, China
- <sup>3</sup> Xiamen Key Laboratory of Rare Earth Photoelectric Functional Materials, Xiamen Institute of Rare Earth Materials, Haixi Institutes, Chinese Academy of Sciences, Xiamen 361021, China
- <sup>4</sup> University of Chinese Academy of Sciences, Beijing 100049, China
- \* Correspondence: yghuang@fjirsm.ac.cn

**Abstract:** Ester hydrates, as the intermediates of the esterification between acid and alcohol, are very short-lived and challenging to be trapped. Therefore, the crystal structures of ester hydrates have rarely been characterized. Herein, we present that the mono-deprotonated ester hydrates  $[\text{CH}_3\text{OSO}_2(\text{OH})_2]^-$ , serving as the template for the self-assembly of a  $\pi$ -stacked boat-shaped macrocycle  $(\text{CH}_3\text{OSO}_2(\text{OH})_2)_{0.67}(\text{CH}_3\text{OSO}_3)_{1.33}@\{[\text{CILCo}^{\text{II}}]_6\}\cdot\text{Cl}_4\cdot 13\text{CH}_3\text{OH}\cdot 9\text{H}_2\text{O}$  (**1**) (L = tris(2-benzimidazolylmethyl) amine), can be trapped in the host by multiple  $\text{NH}\cdots\text{O}$  hydrogen bonds. In the solution of  $\text{CoCl}_2$ , L, and  $\text{H}_2\text{SO}_4$  in MeOH,  $\text{HSO}_4^-$  reacts with MeOH, producing  $[\text{CH}_3\text{OSO}_3]^-$  via the ester hydrate intermediate of  $[\text{CH}_3\text{OSO}_3(\text{OH})_2]^-$ . Both the product and the intermediate serve as the template directing the self-assembly of the  $\pi$ -stacked macrocycle, in which the short-lived ester hydrate is firmly trapped and stabilized, as revealed by single-crystal analysis.

**Keywords:** ester hydrate; self-assembly;  $\pi$ -stacking interaction; hydrogen bonding; intermediate



**Citation:** Wang, B.; Nan, Z.-A.; Li, Q.; Liu, J.; Lu, Z.-X.; Wang, W.; Zhuo, Z.; Li, G.-L.; Huang, Y.-G. Trapping an Ester Hydrate Intermediate in a  $\pi$ -Stacked Macrocycle with Multiple Hydrogen Bonds. *Molecules* **2023**, *28*, 5705. <https://doi.org/10.3390/molecules28155705>

Academic Editor: Michael A. Beckett

Received: 23 June 2023  
Revised: 22 July 2023  
Accepted: 26 July 2023  
Published: 28 July 2023



**Copyright:** © 2023 by the authors. Licensee MDPI, Basel, Switzerland. This article is an open access article distributed under the terms and conditions of the Creative Commons Attribution (CC BY) license (<https://creativecommons.org/licenses/by/4.0/>).

## 1. Introduction

Esters are important chemicals because of their wide applications in a variety of products ranging from medicine to biodiesel [1–3]. Esters can be produced via esterification reactions between the corresponding acids and alcohols via an intermediate state involving two transition states [4,5]. To trap the short-lived intermediate species, some special strategies have to be adopted. Previous reports have demonstrated that reactive species can be stabilized using the cavities of porous materials [6–16]. For instance, air and moisture-reactive white phosphorus can be safely stored in some tetrahedral cages, as demonstrated by Nitschke et al. and Wu et al. [17–19]. Furthermore, various reactive intermediates, including a sulfenic acid [20–22], a selenenic acid [23,24], an S-nitrosothiol [25–27], and a Se-nitrososelenol [28], have been isolated for the “peripheral steric protection” of pre-designed molecular cavities [29]. Inspired by the exceptional functionalities of cavities on stabilizing reactive intermediates, Fujita et al. performed a simple and ubiquitous reaction between an amine and an aldehyde in a porous network and successfully observed a trapped transient hemiaminal via single-crystal X-ray diffraction analysis (SCXRD), which usually is a very short-lived intermediate [30].

Different from the above-mentioned strategies, reactive intermediates may also act as the templates for directing the assembly of molecular cages or macrocycles. As a result, the reactive intermediates may be stabilized and trapped by the resulting assemblies, thus

allowing structural characterizations. Recently, our group started to using the tripodal ligands tris(2-benzimidazolymethyl) amine and tris(2-naphthimidazolymethyl) amine to construct hierarchical assemblies based on  $\pi$ -stacked cages [31–35]. Here, we report the in situ-generated ester hydrate intermediate  $[\text{CH}_3\text{OSO}_2(\text{OH})_2]^-$  templates and the assembly of a boat-shaped  $\pi$ -stacked macrocycle, in which the short-lived ester hydrate is firmly trapped and stabilized, thus enabling the structural determination of the intermediate via single-crystal X-ray analysis.

## 2. Results and Discussion

### 2.1. Trapping the Ester Hydrate Intermediate $[\text{CH}_3\text{OSO}_2(\text{OH})_2]^-$

The esterification between  $\text{H}_2\text{SO}_4$  and  $\text{MeOH}$  involves the attacking of sulfate acid with a nucleophilic  $\text{MeOH}$  molecule to form the ester hydrate intermediate  $\text{CH}_3\text{OSO}(\text{OH})_3$  (Figure 1). The ester hydrate intermediate  $\text{CH}_3\text{OSO}(\text{OH})_3$  is short-lived and challenging to be trapped, and, thus, its crystal structure has not been determined. To trap the intermediate  $[\text{CH}_3\text{OSO}_2(\text{OH})_2]^-$ , we performed esterification between  $\text{H}_2\text{SO}_4$  and  $\text{MeOH}$  in a  $\text{MeOH}$  solution containing cobalt chloride hexahydrate ( $\text{CoCl}_2 \cdot 6\text{H}_2\text{O}$ ), sulfuric acid ( $\text{H}_2\text{SO}_4$ ), and L. We reasoned that assemblies composed of  $[\text{CILCo}^{\text{II}}]^+$  ions can be readily obtained with the templating of the in situ-generated ester hydrate  $[\text{CH}_3\text{OSO}_2(\text{OH})_2]^-$ . Therefore, the intermediate  $[\text{CH}_3\text{OSO}_2(\text{OH})_2]^-$  can be trapped and stabilized due to the confinement of the resulting assembly.

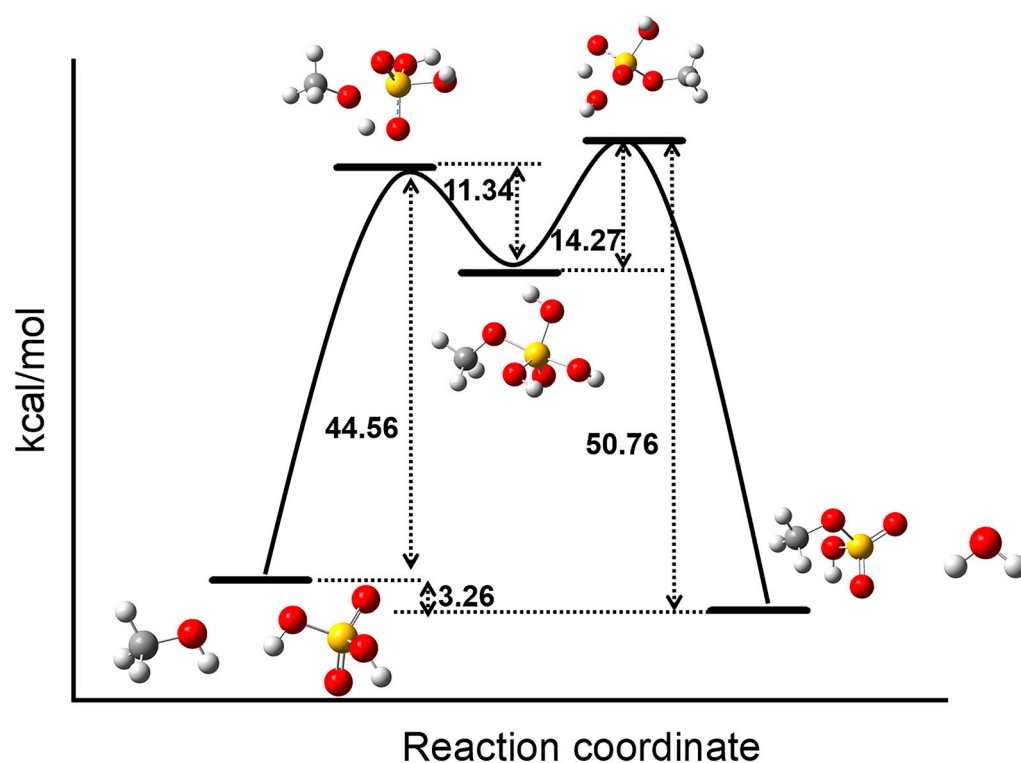


**Figure 1.** Calculated potential energy surface for the reaction pathway of  $\text{MeOH}$  and sulfate acid. Although the formation of the ester hydrate intermediate is endothermic, the overall reaction is exothermic.

To clarify whether the ester hydrate intermediate  $[\text{CH}_3\text{OSO}_2(\text{OH})_2]^-$  was produced and trapped, we performed High-Resolution Mass Spectrometry (HR-MS) analysis on the reactant solution. We successfully identified the species as possibly of  $\{(\text{CH}_3)\text{OSO}_2(\text{OH})_2@[\text{CILCo}^{\text{II}}]_3\}^{2+}$  (identified as  $\{(\text{CH}_3)\text{OSO}_2(\text{OH})_2@[\text{CILCo}^{\text{II}}]_3-\text{H}^++2\text{Cl}^- -2e\}^+$ ) (Figure S1a) and  $\{(\text{CH}_3\text{OSO}_2(\text{OH})_2)(\text{CH}_3\text{OSO}_3)@[\text{CILCo}^{\text{II}}]_3\}^+$  (identified as  $\{(\text{CH}_3\text{OSO}_2(\text{OH})_2)(\text{CH}_3\text{OSO}_3)@[\text{CILCo}^{\text{II}}]_3+\text{Cl}^-+\text{H}^+\}^+$ ) (@: guest at host) (Figure S1b). This result suggests the ester hydrate intermediate was possibly produced and trapped.

Keeping the reactant solution undisturbed at 10 °C for seven days, purple cubic crystals of  $(\text{CH}_3\text{OSO}_2(\text{OH})_2)_{0.67}(\text{CH}_3\text{OSO}_3)_{1.33}@\{[\text{CILCo}^{\text{II}}]_6\}\cdot\text{Cl}_4\cdot 13\text{CH}_3\text{OH}\cdot 9\text{H}_2\text{O}$  (**1**) could be harvested. The successful trapping of the ester hydrate  $[\text{CH}_3\text{OSO}_2(\text{OH})_2]^-$  was further indicated via single-crystal X-ray analysis of compound **1**. The formula of compound **1** was determined using a combination of single-crystal X-ray crystallography (Table S1) and TG analysis (Figure S2). Single-crystal X-ray analysis of compound **1** revealed a  $\pi$ -stacked boat-shaped macrocycle composed of six  $[\text{CILCo}^{\text{II}}]^+$  ions, in which the ester hydrate intermediate  $[\text{CH}_3\text{OSO}_2(\text{OH})_2]^-$  and the esterification product  $[\text{CH}_3\text{OSO}_3]^-$  were trapped in a ratio of 1:2.

Compound **1** crystallized in the trigonal space group  $R\bar{3}$ , with the asymmetric unit containing one  $[\text{CILCo}^{\text{II}}]^+$ ,  $1/9$   $[\text{CH}_3\text{OSO}_2(\text{OH})_2]^-$ ,  $2/9$   $[\text{CH}_3\text{OSO}_3]^-$ ,  $2/3$   $\text{Cl}^-$ ,  $13/6$   $\text{CH}_3\text{OH}$ , and some disordered  $\text{H}_2\text{O}$  molecules. In  $[\text{CILCo}^{\text{II}}]^+$ , the central  $\text{Co}^{2+}$  bound to four N atoms from the same L ligand and one  $\text{Cl}^-$  in a trigonal-bipyramidal geometry. The tripodal  $[\text{CILCo}^{\text{II}}]^+$  featured its three identical benzimidazolymethyl arms, which were potential active sites for intermolecular  $\pi$ -stacking interactions (Figure 2a). In compound **1**, each  $[\text{CILCo}^{\text{II}}]^+$  associated with its two neighbors through  $\pi\cdots\pi$  interactions, with centroid distances for phenyl $\cdots$ imidazole, phenyl $\cdots$ phenyl, and imidazole $\cdots$ imidazole of 3.732, 3.809, and 4.044 Å, respectively. As a result, the boat-shaped macrocycle formed. Each vertex of the macrocycle was occupied by  $[\text{CILCo}^{\text{II}}]^+$  and each edge was composed of a pair of  $\pi$ -stacked benzimidazolymethyl arms. Each macrocycle captured two guest molecules via multiple host–guest  $\text{NH}\cdots\text{O}$  ( $d_{\text{H}\cdots\text{O}}$  in the range of 1.728–2.141 Å) hydrogen bonds ( $[(\text{CH}_3\text{OSO}_2(\text{OH})_2)]^-$  and  $[\text{CH}_3\text{OSO}_3]^-$  existed statistically in a ratio of 1:2) (Figure 2b and Figure S3). Both the  $[\text{CH}_3\text{OSO}_2(\text{OH})_2]^-$  and  $[\text{CH}_3\text{OSO}_3]^-$ , located on the  $C_3$ -axis, and the  $[\text{CH}_3\text{OSO}_2(\text{OH})_2]^-$  intermediate were highly disordered (note: because of the levels of disorder, the interpretation of these data is a hypothesis, with levels of certainty lower than for the remainder of the structure). HR-MS analysis was also performed on the methanol solution of the crystal of compound **1**. The species of  $\{(\text{CH}_3\text{OSO}_2(\text{OH})_2)^-\}$  (identified as  $\{(\text{CH}_3\text{OSO}_2(\text{OH})_2+\text{Na}^++2\text{NH}_4^+-\text{H}^+)\}^+$  (Figure S1c) and  $\{(\text{CH}_3\text{OSO}_2(\text{OH})_2)(\text{CH}_3\text{OSO}_3)\}^{2-}$  (identified as  $\{(\text{CH}_3\text{OSO}_2(\text{OH})_2)(\text{CH}_3\text{OSO}_3)+3\text{NH}_4^++\text{H}^++e\}^+$  (Figure S1d) could be identified, which was consistent with the X-ray structure analysis. Therefore, both the  $[\text{CH}_3\text{OSO}_2(\text{OH})_2]^-$  intermediate and the  $[\text{CH}_3\text{OSO}_3]^-$  product were unambiguously produced and trapped. Each macrocycle further associated with its six neighbors (Figure 2c) for the rest of the benzimidazolymethyl arm, giving rise to a three-dimensional (3D) network. If treating the macrocycle as node and the  $\pi$ -stacked pair of benzimidazolymethyl arms as linker, the 3D network can be simplified as an  $\alpha$ - $\text{P}_0$  net (Figure 2d). Alternatively, the 3D network can be simplified as a  $\text{pcu-h}$  net if treating  $[\text{CILCo}^{\text{II}}]^+$  as node and the  $\pi$ -stacked pair of benzimidazolymethyl arms as linker (Figure S4) [36].

## 2.2. Physical-Property Characterization of Compound 1

The phase purity of compound **1** was confirmed via the powder X-ray diffraction pattern (PXRD) measurement (Figure S5). In the infra-red (IR) spectrum of compound **1**, the absorption band at  $1395\text{ cm}^{-1}$  can be assigned to  $\nu_{(\text{S}=\text{O})}$  and the band at  $1022\text{ cm}^{-1}$  can be assigned to  $\nu_{(\text{C}-\text{O})}$  [37,38] (Figure 3a). The existence of  $\text{S}^{\text{VI}}$  was confirmed using the X-ray photoelectron spectroscopy (XPS) study. The observed peaks at 168.15 and 169.25 eV corresponded to  $\text{S}^{\text{VI}} 2p_{3/2}$  and  $\text{S}^{\text{VI}} 2p_{1/2}$ , respectively [39,40] (Figure 3b). A temperature-dependent magnetization study of compound **1** was also performed under 1 kOe field in the 2–300 K range. The  $\chi_m T$  value of  $14.95\text{ cm}^3\text{ K mol}^{-1}$  at 300 K was higher than the spin-only value of six isolated high-spin  $\text{Co}^{\text{II}}$  ions ( $11.25\text{ cm}^3\text{ mol}^{-1}\text{ K}$ ) (Figure 3c) [41–43]. This result implies an obvious unquenched orbital contribution. Upon cooling, the  $\chi_m T$  value kept almost constant until 10 K, and then began to decrease, reaching a value of  $12.14\text{ cm}^3\text{ mol}^{-1}\text{ K}$  at 2 K, implying very weak antiferromagnetic couplings between  $\text{Co}^{\text{II}}$  ions. In the range of 300–2 K, the magnetic susceptibility data followed Curie–Weiss law, giving  $\theta = -1.13\text{ K}$  and  $C = 14.79\text{ cm}^3\text{ K mol}^{-1}$ , confirming the dominant weak antiferromagnetic interactions. To give further insights into the magnetism of compound **1**,

the field-dependent magnetizations were measured. The magnetization increased slowly with the increasing field and reached a value of  $19.10 \text{ N}\beta$  at  $80 \text{ kOe}$  without obvious hysteresis (Figure 3d), which is consistent with the weak antiferromagnetic couplings between  $\text{Co}^{\text{II}}$  ions [44,45].

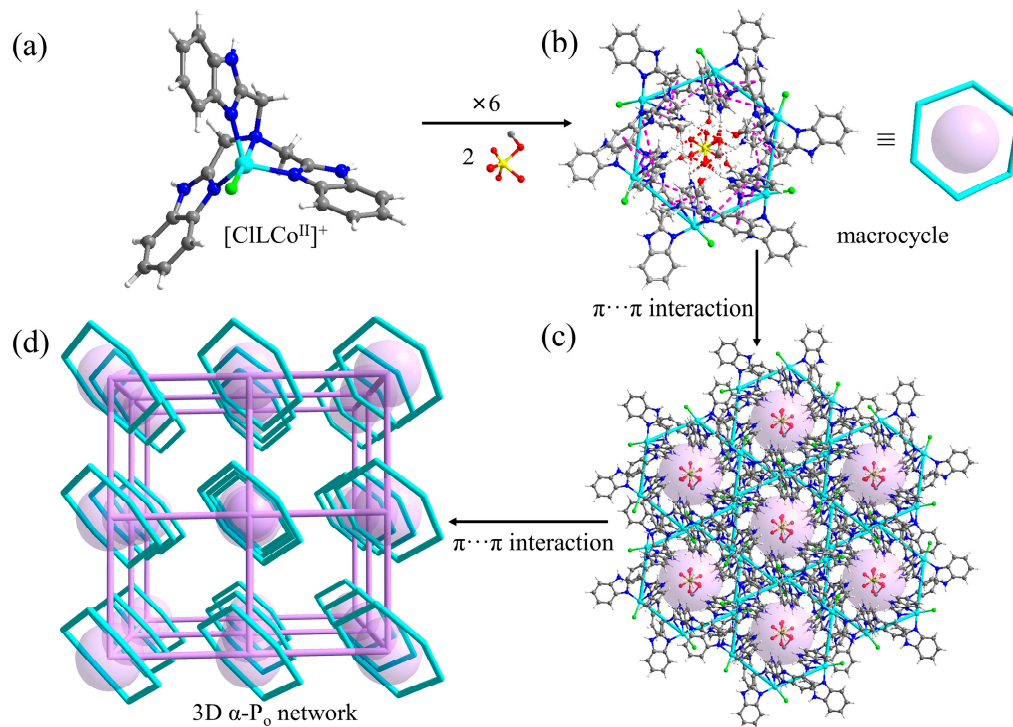


**Figure 2.** Hierarchical structure of compound 1. (a) Structure of  $[\text{CILCo}^{\text{II}}]^+$ . (b) Top view of the boat-shaped macrocycle of compound 1. (c) View of each macrocycle associating with its six neighbors. (d) The 3D  $\alpha\text{-P}_0$  network of compound 1.

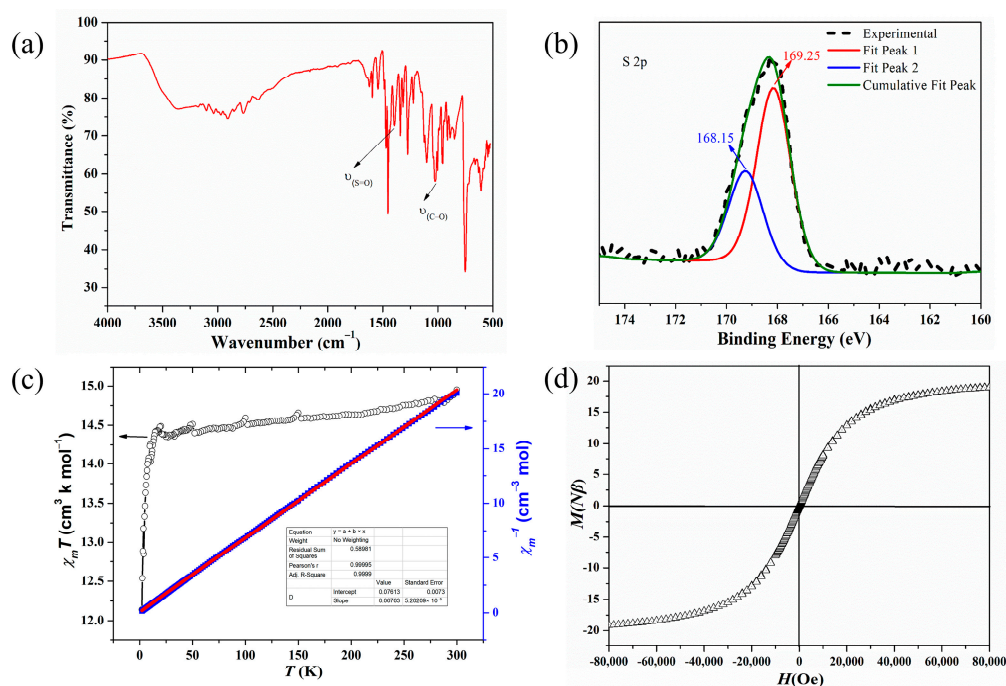


**Figure 3.** (a) IR spectrum of compound 1. (b) XPS of the crystalline sample of 1. (c) The plot of  $\chi_m T$ – $T$  and  $\chi_m^{-1} T$ – $T$  of compound 1. (d) The plot of  $M$ – $H$  of compound 1.

### 3. Experimental Methods

#### 3.1. Materials and Physical Measurements

The ligand tris(2-benzimidazolylmethyl) amine (L) was synthesized according to the procedure reported in the literature [46], and all the other reagents were commercially obtained and used without further purification. Powder X-ray diffraction (PXRD, Miniflex 600, Akishima, Rigaku, Tokyo, Japan) patterns were performed on a Rigaku Miniflex 600 diffractometer with Cu-K $\alpha$  radiation using flat plate geometry. High Resolution Mass Spectrometry (HR-MS, Impact II UHR-TOF, Bruker, Billerica, MA, USA) measurements were performed on a DECAX-30000 LCQ Deca XP system. X-ray photoelectron spectroscopy (XPS, Axis Supra, Shimadzu, Manchester, United Kingdom) studies were performed on an AXIS SUPRA Kratos system and the C1s line at 284.8 eV was used as the binding energy reference. Thermogravimetric analysis (TGA/DSC 1, Mettler Toledo, Zurich, Switzerland) was performed on a Mettler-Toledo TGA/DSC 1 system with a heating rate of 10 K/min under an argon atmosphere. Fourier-transform infrared (FTIR, Nicolet iS 50, Thermo Fisher, Waltham, MA, USA) spectra were recorded in the range of 500–4000 cm<sup>-1</sup> on a Thermo Nicolet iS50 FT-IR spectrometer at room temperature. Magnetic measurements (MPMS-5S SQUID, Quantum Design, San Diego, CA, USA) were performed on an MPMS-5S SQUID magnetometer.

#### 3.2. Synthesis of Compound 1

Synthesis of (CH<sub>3</sub>OSO<sub>2</sub>(OH))<sub>0.66</sub>(CH<sub>3</sub>OSO<sub>3</sub>)<sub>1.33</sub>@{[CILCo<sup>II</sup>]<sub>6</sub>}.Cl<sub>4</sub>.13CH<sub>3</sub>OH.9H<sub>2</sub>O (**1**): A mixture of L (4.07 g, 0.01 mol), CoCl<sub>2</sub>·6H<sub>2</sub>O (Alfa, 4.76 g, 0.02 mol), and trace amounts of aqueous solution of H<sub>2</sub>SO<sub>4</sub> (Sinopharm, Beijing, China, 20  $\mu$ L, 0.001 mmol) in 500 mL methanol (Hushi) was stirred at room temperature for 5 min. After that, the insoluble matters were removed via filtration. The resulting solution was kept undisturbed at 10 °C. Purple cubic crystals of compound **1** were obtained within seven days.

#### 3.3. Crystallography

Single-crystal X-ray data were harvested on a Bruker D8 Venture diffractometer with Mo-K $\alpha$  radiation at 200 K. Structures were solved using intrinsic phasing method with SHELXT and refined via the full-matrix least-squares technique on F<sup>2</sup> with SHELXTL 2014 program [47]. The graphical user interface for the solving and refining process adopted Olex2 software [48]. In the process of solving crystals, some reasonable restriction commands such as DFIX, SIMU, and OMIT were used. All the H atoms were geometrically generated and refined using a riding model. The X-ray crystallographic coordinates for structures reported in this article have been deposited at the Cambridge Crystallographic Data Centre (CCDC) under deposition numbers 2271453. These data can be obtained free of charge from The Cambridge Crystallographic Data Centre via [www.ccdc.cam.ac.uk/data\\_request/cif](http://www.ccdc.cam.ac.uk/data_request/cif) (accessed on 22 June 2023). Detailed crystallographic data are listed in Table S1.

#### 3.4. Computational Methods

We calculated the complete reaction pathway of methanol and vitriol (Figure 1). The geometry structures and the frequency calculations of reactants, products, and intermediate structures, as well as transition-structures (TS) have been optimized using the M062X method and the 6-31G\* basis set [49]. Using the same method and basis set, the vibrational frequency calculations were carried out to confirm the local minima intermediate structure and the TS (one negative eigenvalue) on the potential energy surface (PES). The M062X method and the 6-31G\* basis set were employed to calculate the intrinsic reaction coordinates (IRCs) [50], verifying that the TS were indeed the lowest saddle points for the expected structure connecting the reaction path. All calculations were performed using Gaussian 16 program [51].

#### 4. Conclusions

In conclusion, the reactive ester hydrate intermediate  $[\text{CH}_3\text{OSO}_2(\text{OH})_2]^-$  has been successfully trapped and stabilized as the template for directing the assembly of  $\pi$ -stacked boat-shaped macrocycles. The intermediate is firmly trapped in the macrocycle by multiple  $\text{NH}\cdots\text{O}$  hydrogen bonds. This achievement allowed for the structural determination of the intermediate using single-crystal X-ray analysis. This strategy for stabilizing reactive species may be planted to other systems, and, thus, provides a new means of giving insights into the structural transformations that occur during chemical reactions.

**Supplementary Materials:** The following supporting information can be downloaded at: <https://www.mdpi.com/article/10.3390/molecules28155705/s1>, Table S1: Crystallographic data of the synthetic compound **1**; Figure S1. HR-MS of the reactant solution and the solution of compound **1** in methanol. (a) HR-MS of  $\{(\text{CH}_3\text{OSO}_2(\text{OH})_2)@[\text{CILCo}^{\text{II}}]_3-\text{H}^++2\text{Cl}^- - 2e\}^+$  identified from the reactant solution. (b) HR-MS of  $\{(\text{CH}_3\text{OSO}_2(\text{OH})_2)(\text{CH}_3\text{OSO}_3)@[\text{CILCo}^{\text{II}}]_3+\text{Cl}^- +\text{H}^+\}^+$  identified from the reactant solution. (c) HR-MS of  $\{(\text{CH}_3\text{OSO}_2(\text{OH})_2)+\text{Na}^++2\text{NH}_4^+ -\text{H}^+\}^+$  identified from the solution of compound **1** in methanol. (d) HR-MS of  $\{(\text{CH}_3\text{OSO}_2(\text{OH})_2)(\text{CH}_3\text{OSO}_3)+3\text{NH}_4^++\text{H}^++e\}^+$  identified from the solution of compound **1** in methanol; Figure S2: TGA for compound **1**; Figure S3. Side view of the structure of the boat-shaped macrocycle templating by  $[\text{CH}_3\text{OSO}_2(\text{OH})_2]^-$  and  $[\text{CH}_3\text{OSO}_3]^-$  in compound **1**. (inset: structure of the ester hydrate  $[\text{CH}_3\text{OSO}_2(\text{OH})_2]^-$  in compound **1**); Figure S4. The pcu-h network of compound **1** when treating  $[\text{CILCo}^{\text{II}}]^+$  as node and the  $\pi$ -stacked pair of benzimidazolymethyl arms as linker; Figure S5: PXRD patterns of compound **1**.

**Author Contributions:** B.W. performed experiments and wrote the paper. Z.-A.N. directed the compound characterization and data analysis. Q.L. performed the theoretical calculation. J.L. and Z.-X.L. collected data. Z.Z., W.W. and G.-L.L. contributed to interpreting the data. Y.-G.H. conceived the project. All authors have read and agreed to the published version of the manuscript.

**Funding:** This research was funded by the National Natural Science Found (NNSF) of China (92261109 and 21901242), the NSF of Fujian Province (2020J05080), the NSF of Xiamen (3502Z20206080), the Fujian Science and Technology Innovation Laboratory for Optoelectronic Information of China (2021ZR110), the Recruitment Program of Global Youth Experts, and the Youth Innovation Promotion Association.

**Institutional Review Board Statement:** Not applicable.

**Informed Consent Statement:** Not applicable.

**Data Availability Statement:** All data related to this study are presented in this publication.

**Conflicts of Interest:** The authors declare no conflict of interest.

**Sample Availability:** Samples are available from the authors.

#### References

1. Glisic, S.B.; Pajnik, J.M.; Orlović, A.M. Process and techno-economic analysis of green diesel production from waste vegetable oil and the comparison with ester type biodiesel production. *Appl. Energy* **2016**, *170*, 176–185. [CrossRef]
2. Egle, S.; Violeta, M. Biodiesel fuel synthesis by transesterification of triglycerides with carboxylate esters of low molecular weight. *Rev. Chem. Eng.* **2021**, *37*, 259–276.
3. Chen, H.; Zhang, R.; Luo, R.-H.; Yang, L.-M.; Wang, R.-R.; Hao, X.-J.; Zheng, Y.-T. Anti-HIV activities and mechanism of 12-*o*-tricosanoylphorbol-20-acetate, a novel phorbol ester from *Ostodes katharinae*. *Molecules* **2017**, *22*, 1498. [CrossRef]
4. Kirumakki, S.R.; Nagaraju, N.; Chary, K.V.R. Esterification of alcohols with acetic acid over zeolites H $\beta$ , HY and HZSM5. *Appl. Catal. A-Gen.* **2006**, *299*, 185–192.
5. Miao, S.; Shanks, B.H. Mechanism of acetic acid esterification over sulfonic acid-functionalized mesoporous silica. *J. Catal.* **2011**, *279*, 136–143. [CrossRef]
6. Iwasawa, T.; Hooley, R.J.; Rebek, J., Jr. Stabilization of labile carbonyl addition intermediates by a synthetic receptor. *Science* **2007**, *317*, 493–496.
7. Yoshizawa, M.; Kusukawa, T.; Fujita, M.; Yamaguchi, K. Ship-in-a-bottle synthesis of otherwise labile cyclic trimers of siloxanes in a self-assembled coordination cage. *J. Am. Chem. Soc.* **2000**, *122*, 6311–6312. [CrossRef]
8. Liu, Q.-K.; Ma, J.P.; Dong, Y.-B. Adsorption and separation of reactive aromatic isomers and generation and stabilization of their radicals within cadmium(II)-triazole metal-organic confined space in a single-crystal-to-single-crystal fashion. *J. Am. Chem. Soc.* **2010**, *132*, 7005–7017. [CrossRef]

9. Ning, G.-H.; Inokuma, Y.; Fujita, M. Stable encapsulation of acrylate esters in networked molecular capsules. *Chem.-Asian J.* **2014**, *9*, 466–468. [[PubMed](#)]
10. Schwarzmaier, C.; Schindler, A.; Heindl, C.; Scheuermayer, S.; Peresyphkina, E.V.; Virovets, A.V.; Neumeier, M.; Gschwind, R.; Scheer, M. Stabilization of tetrahedral P<sub>4</sub> and As<sub>4</sub> molecules as guests in polymeric and spherical environments. *Angew. Chem. Int. Ed.* **2013**, *52*, 10896–10899. [[CrossRef](#)]
11. Kaanumalle, L.S.; Nithyanandhan, J.; Pattabiraman, M.; Jayaraman, N.; Ramamurthy, V. Water-soluble dendrimers as photochemical reaction media: Chemical behavior of singlet and triplet radical pairs inside dendritic reaction cavities. *J. Am. Chem. Soc.* **2004**, *126*, 8999–9006. [[CrossRef](#)]
12. Eelkema, R.; Maeda, K.; Odell, B.; Anderson, H.L. Radical Cation Stabilization in a Cucurbituril Oligoaniline Rotaxane. *J. Am. Chem. Soc.* **2007**, *129*, 12384–12385. [[CrossRef](#)]
13. Liu, Y.; Shi, J.; Chen, Y.; Ke, C.-F. A polymeric pseudorotaxane constructed from cucurbituril and aniline, and stabilization of its radical cation. *Angew. Chem. Int. Ed.* **2008**, *47*, 7293–7296. [[CrossRef](#)]
14. Shi, J.; Chen, Y.; Wang, Q.; Liu, Y. Construction and efficient radical cation stabilization of cyclodextrin/aniline polypseudorotaxane and its conjugate with carbon nanotubes. *Adv. Mater.* **2010**, *22*, 2575–2578. [[CrossRef](#)] [[PubMed](#)]
15. Wei, W.; Li, W.L.; Li, Z.F.; Su, W.P.; Hong, M.C. Stabilization and controlled release of reactive molecules by solid-state van der Waals capsules. *Chem.-Eur. J.* **2013**, *19*, 468–472. [[CrossRef](#)] [[PubMed](#)]
16. Galan, A.; Ballester, P. Stabilization of reactive species by supramolecular encapsulation. *Chem. Soc. Rev.* **2016**, *45*, 1720–1737. [[CrossRef](#)] [[PubMed](#)]
17. Mal, P.; Breiner, B.; Rissanen, K.; Nitschke, J.R. White phosphorus is air-stable within a self-assembled tetrahedral capsule. *Science* **2009**, *324*, 1697–1699. [[CrossRef](#)]
18. Jiao, T.Y.; Chen, L.; Yang, D.; Li, X.; Wu, G.C.; Zeng, P.M.; Zhou, A.K.; Yin, Q.; Pan, Y.J.; Wu, B.; et al. Trapping white phosphorus within a purely organic molecular container produced by imine condensation. *Angew. Chem. Int. Ed.* **2017**, *56*, 14545–14550. [[CrossRef](#)] [[PubMed](#)]
19. Yang, D.; Zhao, J.; Yu, L.; Lin, X.S.; Zhang, W.Y.; Ma, H.W.; Gogoll, A.; Zhang, Z.B.; Wang, Y.Y.; Yang, X.-J.; et al. Air- and light-stable P<sub>4</sub> and As<sub>4</sub> within an anion-coordination-based tetrahedral cage. *J. Am. Chem. Soc.* **2017**, *139*, 5946–5951. [[CrossRef](#)]
20. Sano, T.; Masuda, R.; Sase, S.; Goto, K. Isolable small-molecule cysteine sulfenic acid. *Chem. Commun.* **2021**, *57*, 2479. [[CrossRef](#)] [[PubMed](#)]
21. Kumar, M.R.; Farmer, P.J. Trapping reactions of the sulfenyl and sulfinyl tautomers of sulfenic acids. *ACS Chem. Biol.* **2017**, *12*, 474–478. [[CrossRef](#)] [[PubMed](#)]
22. Liu, C.T.; Benkovic, S.J. Capturing a sulfenic acid with arylboronic acids and benzoxaborole. *J. Am. Chem. Soc.* **2013**, *135*, 14544–14547. [[CrossRef](#)]
23. Saiki, T.; Goto, K.; Okazaki, R. Isolation and X-ray crystallographic analysis of a stable selenenic acid. *Angew. Chem. Int. Ed.* **1997**, *36*, 2223. [[CrossRef](#)]
24. Goto, K.; Saiki, T.; Akine, S.; Kawashima, T.; Okazaki, R. Synthesis and reactions of conformational isomers of a stable selenenic acid bearing a bridged calix [6] arene framework. *Heteroat. Chem.* **2001**, *12*, 195–197.
25. Kei, G.; Yoko, H.; Yusuke, T.; Takayuki, K.; Gaku, Y.; Nozomi, T.; Shigeru, N. Synthesis, structure, and reactions of the first stable aromatic S-nitrosothiol bearing a novel dendrimer-type steric protection group. *Chem. Lett.* **2001**, *30*, 1204–1205.
26. Goto, K.; Hino, Y.; Kawashima, T.; Kaminaga, M.; Yano, E.; Yamamoto, G.; Takagic, N.; Nagase, S. Synthesis and crystal structure of a stable S-nitrosothiol bearing a novel steric protection group and of the corresponding S-nitrothiol. *Tetrahedron Lett.* **2000**, *41*, 8479–8483. [[CrossRef](#)]
27. Okazaki, R.; Goto, K. Synthesis of highly reactive organosulfur compounds. *Heteroat. Chem.* **2002**, *13*, 414–418. [[CrossRef](#)]
28. Shimada, K.; Goto, K.; Kawashima, T.; Takagi, N.; Choe, Y.-K.; Nagase, S. Isolation of a Se-nitrososelenol: A new class of reactive nitrogen species relevant to protein Se-nitrosation. *J. Am. Chem. Soc.* **2004**, *126*, 13238–13239.
29. Goto, K.; Kawashima, T. Nanoscale molecular cavities for stabilization of highly reactive species. *J. Syn. Org. Chem. Jpn.* **2005**, *63*, 1157–1170. [[CrossRef](#)]
30. Kawamichi, T.; Haneda, T.; Kawano, M.; Fujita, M. X-ray observation of a transient hemiaminal trapped in a porous network. *Nature* **2009**, *461*, 633–635. [[CrossRef](#)]
31. Li, S.; Li, G.-L.; Wang, W.; Liu, Y.; Cao, Z.-M.; Cao, X.-L. A 2D metal-organic framework interpenetrated by a 2D supramolecular framework assembled by CH/π interactions. *Inorg. Chem. Commun.* **2021**, *130*, 108705. [[CrossRef](#)]
32. Li, L.-L.; Huang, M.; Chen, T.; Xu, X.-F.; Zhuo, Z.; Wang, W.; Huang, Y.-G. A porous π-stacked self-assembly of cup-shaped palladium complex for iodine capture. *Molecules* **2023**, *28*, 2881. [[CrossRef](#)]
33. Chen, T.; Li, S.; Wang, Z.-B.; Wu, Z.-Y.; Huang, M.; Wang, W.; Zhuo, Z.; Huang, Y.-G. Iodine uptake enhanced electrical conductivity by a metal-organic framework bearing nanotube array of π-stacked columns. *J. Mol. Struct.* **2023**, *1289*, 135858. [[CrossRef](#)]
34. Li, G.-L.; Zhuo, Z.; Wang, B.; Cao, X.-L.; Su, H.-F.; Wang, W.; Huang, Y.-G.; Hong, M.-C. Constructing π-stacked supramolecular cage based hierarchical self-assemblies via π···π stacking and hydrogen bonding. *J. Am. Chem. Soc.* **2021**, *143*, 10920–10929. [[CrossRef](#)]
35. Liu, J.; Lu, Z.-X.; Wu, F.-F.; Wang, B.; Cao, X.-L.; Wang, W.; Zhuo, Z.; Li, Q.-H.; Huang, Y.-G. A chiral SrSi<sub>2</sub> (srs) superstructure constructed by a dual interaction system showing isotropic electrical conductivity. *Chin. Chem. Lett.* **2022**, *1001*, 108100. [[CrossRef](#)]

36. Xie, J.-H.; Tan, Y.-Z.; Li, Z.-H.; Zhou, Q.; Ou, G.-C. Synthesis, crystal structures, and theoretical calculations of two diverse three-dimensional hybrid materials based on polyoxoanions bridging macrocyclic copper/nickel complex. *Inorg. Nano-Met. Chem.* **2021**, *51*, 889–895. [[CrossRef](#)]
37. Simon, A.; Kriegsmann, H. Schwingungsspektren von alkylderivaten der schwefligen säure, I. Mitteil.: Raman- und IR-spektren der alkali-methansulfonate. *Chem. Ber.* **1956**, *89*, 1718–1726. [[CrossRef](#)]
38. Chihara, G. Characteristic infrared absorption band of organic sulfate esters. *Chem. Pharm. Bull.* **1958**, *6*, 114. [[CrossRef](#)]
39. Zhang, L.; Li, Z.; Yang, Y.; Zhou, Y.; Li, J.; Si, L.; Kong, B. Research on the composition and distribution of organic sulfur in coal. *Molecules* **2016**, *21*, 630. [[CrossRef](#)]
40. Wibowo, E.S.; Park, B.-D. Chemical and thermal characteristics of ion-exchanged lignosulfonate. *Molecules* **2023**, *28*, 2755. [[CrossRef](#)]
41. Yang, E.C.; Hendrickson, D.N.; Wernsdorfer, W.; Nakano, M.; Zakharov, L.N.; Sommer, R.D.; Rheingold, A.L.; Ledezma-Gairaud, M.; Christou, G. Cobalt single-molecule magnet. *J. Appl. Phys.* **2002**, *91*, 7382–7384. [[CrossRef](#)]
42. Ostrovsky, S.M.; Falk, K.; Pelikan, J.; Brown, D.A.; Tomkowicz, Z.; Haase, W. Orbital angular momentum contribution to the magneto-optical behavior of a binuclear cobalt(II) complex. *Inorg. Chem.* **2006**, *2*, 688–694.
43. Matsuoka, R.; Yoshimoto, T.; Kitagawa, Y.; Kusamoto, T. Structural and Magnetic Studies on Nickel(II) and Cobalt(II) Complexes with Polychlorinated Diphenyl(4-pyridyl)methyl Radical Ligands. *Molecules* **2021**, *26*, 5596. [[CrossRef](#)]
44. Guo, L.R.; Zhu, F.; Chen, Y.; Li, Y.Z.; Zheng, L.M. Layered copper compounds based on 4-(3-bromothiényl) phosphonate (BTP): Weak ferromagnetism observed in  $[\text{Cu}_2(4,4'\text{-bpy})_{0.5}(\text{BTP})_2]\cdot\text{H}_2\text{O}$ . *Dalton Trans.* **2009**, *40*, 8548–8554. [[CrossRef](#)]
45. Azuma, M.; Kaimori, S.; Takano, M. High-pressure synthesis and magnetic properties of layered double perovskites  $\text{Ln}_2\text{CuMO}_6$  (Ln = La, Pr, Nd, and Sm; M = Sn and Zr). *Chem. Mater.* **1998**, *10*, 3124–3130. [[CrossRef](#)]
46. Zhang, S.R.; Du, D.Y.; Qin, J.S.; Bao, S.J.; Li, S.L.; He, W.W.; Lan, Y.Q.; Shen, P.; Su, Z.M. A fluorescent sensor for highly selective detection of nitroaromatic explosives based on a 2D, extremely stable, metal–organic framework. *Chem. Eur. J.* **2014**, *20*, 3589–3594. [[CrossRef](#)]
47. Sheldrick, G.M. SHELXTL-integrated space-group and crystal-structure determination. *Acta Crystallogr.* **2015**, *A71*, 3–8.
48. Dolomanov, O.V.; Bourhis, L.J.; Gildea, R.J.; Howard, J.A.K.; Puschmann, H. OLEX2: A complete structure solution, refinement and analysis program. *J. Appl. Cryst.* **2009**, *42*, 339–341. [[CrossRef](#)]
49. Zhao, Y.; González-García, N.; Truhlar, D.G. Benchmark database of barrier heights for heavy atom transfer, nucleophilic substitution, association, and unimolecular reactions and its use to test theoretical methods. *J. Phys. Chem. A* **2005**, *109*, 2012–2018. [[CrossRef](#)]
50. Gonzalez, C.; Schlegel, H.B. Reaction path following in mass-weighted internal coordinates. *J. Phys. Chem.* **1990**, *94*, 5523–5527. [[CrossRef](#)]
51. Frisch, M.J.; Trucks, G.W.; Schlegel, H.B.; Scuseria, G.E.; Robb, M.A.; Cheeseman, J.R.; Scalmani, G.; Barone, V.; Petersson, G.A.; Nakatsuji, H.; et al. *Gaussian 16 Rev. B.01*; Gaussian Inc.: Wallingford, CT, USA, 2016.

**Disclaimer/Publisher's Note:** The statements, opinions and data contained in all publications are solely those of the individual author(s) and contributor(s) and not of MDPI and/or the editor(s). MDPI and/or the editor(s) disclaim responsibility for any injury to people or property resulting from any ideas, methods, instructions or products referred to in the content.